nature chemical biology

ARTICLES

https://doi.org/10.1038/s41589-019-0447-7

Lipid droplets can promote drug accumulation and activation

Ramin Dubey[1], Craig E. Stivala[2,3], Huy Quoc Nguyen[3], Young-Hwa Goo[4], Antoni Paul[4], Jan E. Carette[5], Barry M. Trost[2] and Rajat Rohatgi[1,6*]

Genetic screens in cultured human cells represent a powerful unbiased strategy to identify cellular pathways that determine drug efficacy, providing critical information for clinical development. We used insertional mutagenesis-based screens in haploid cells to identify genes required for the sensitivity to lasonolide A (LasA), a macrolide derived from a marine sponge that kills certain types of cancer cells at low nanomolar concentrations. Our screens converged on a single gene, *LDAH*, encoding a member of the metabolite serine hydrolase family that is localized on the surface of lipid droplets. Mechanistic studies revealed that LasA accumulates in lipid droplets, where it is cleaved into a toxic metabolite by LDAH. We suggest that selective partitioning of hydrophobic drugs into the oil phase of lipid droplets can influence their activation and eventual toxicity to cells.

Small molecules derived from natural sources have been an invaluable resource for the discovery of new drugs and new tools to study a variety of cellular processes. Natural products have complex and diverse structures with multiple stereocenters, allowing them to interact with and alter the function of cellular proteins with high selectivity. However, understanding the proteins and pathways that mediate cellular responses to natural products can be challenging because of their low abundances and often difficult, multistep chemical syntheses. Genetic screens in cultured human cells, now made routine by the use of haploid cell lines and CRISPR-mediated gene editing, have emerged as powerful methods to discover both the mechanism of action of drugs and the pathways that mediate drug uptake and metabolism. For anticancer applications, this information can identify cellular factors that mediate both de novo and acquired resistance, and thus identify predictive biomarkers to select the tumor types and patients that would derive the greatest benefit from the drug.

Lasonolide A (**1**) (hereafter LasA, Fig. 1a) is a polyketide-derived macrolide isolated from a marine sponge (*Forcepia*) found in the Gulf of Mexico[1,2]. LasA has been considered a good candidate for development as an anticancer drug because it kills cancer cell lines at low nanomolar concentrations and has a unique cytotoxicity profile when tested against the National Cancer Institute (NCI-60) cell panel[1]. LasA has an unusual biphasic effect on cells. Within minutes, it causes loss of cell adhesion, cell blebbing and premature chromosome condensation, effects that are reversible with drug withdrawal[3,4]. Longer treatment leads to irreversible toxicity. While the cellular target of LasA has not been conclusively identified, it triggers protein hyperphosphorylation in cells and has been implicated in the activation of multiple kinases, including PKC, MAPKs and c-RAF[3–5]. Taking advantage of our recent total synthesis of LasA[6], we used genetic screens in a haploid human cell line (Hap1)[7–9] to uncover cellular mechanisms that mediate sensitivity to LasA. The results of our screen, with subsequent mechanistic follow-up, revealed that LasA accumulates in lipid droplets, where it is hydrolyzed into a toxic metabolite by an orphan serine hydrolase enzyme. We suggest that lipid droplets can influence the efficacy of small-molecule drugs by providing both a depot for hydrophobic molecules and a complement of enzymes for drug metabolism. It may be possible to harness such lipid droplet-based mechanisms to increase both drug efficacy and selectivity.

Results

Screens to identify genes required for LasA toxicity. LasA[6] was toxic to Hap1 cells, with an IC_{50} (the concentration causing a 50% inhibition of viability compared to untreated cells) of ~20 nM (Fig. 1b). LasA is composed of a macrocyclic ring and a side chain (Fig. 1a). A series of lasonolides (C–G) have been purified from *Forcepia*, which have the same macrocyclic ring but vary in the structure of the side chain[2]. The toxicity of LasA was sensitive to its chemical structure, suggesting that it interacts with specific protein targets in cells. Movement of a double bond from an endocyclic to an exocyclic position in Ces-73 (**2**) increased the IC_{50} to ~160 nM and expansion of the macrocycle, in Ces-24a (**3**) and Ces-24b (**4**), abolished toxicity (Fig. 1a,b).

We conducted genetic screens in Hap1 cells to identify genes required for cellular sensitivity to LasA and Ces-73, similarly to how we previously identified genes required for cellular sensitivity to doxorubicin[9]. Hap1 cells have a near-haploid genome, which enables the generation of null alleles for most genes by insertional mutagenesis[10]. A library of ~100 million mutagenized Hap1 cells was created by random insertions of a gene-trap cassette delivered using a retrovirus. The entire population was then treated with either LasA at 80 nM or Ces-73 at 400 nM, concentrations that are expected to kill >99% of cells (the IC_{99}). Surviving cells, presumably carrying inactivating insertions in genes required for drug sensitivity, were isolated and the positions of retroviral insertions mapped by deep sequencing (Supplementary Fig. 1). Both screens converged on the finding that inactivating insertions in *LDAH* (lipid droplet-associated hydrolase or *C2ORF43*) made cells resistant to LasA (Fig. 1c and Supplementary Fig. 2a).

[1]Department of Biochemistry, Stanford University School of Medicine, Stanford, CA, USA. [2]Department of Chemistry, Stanford University, Stanford, CA, USA. [3]Genentech, South San Francisco, CA, USA. [4]Department of Molecular and Cellular Physiology, Albany Medical College, Albany, NY, USA. [5]Department of Microbiology and Immunology, Stanford University School of Medicine, Stanford, CA, USA. [6]Department of Medicine, Stanford University School of Medicine, Stanford, CA, USA. *e-mail: rrohatgi@stanford.edu

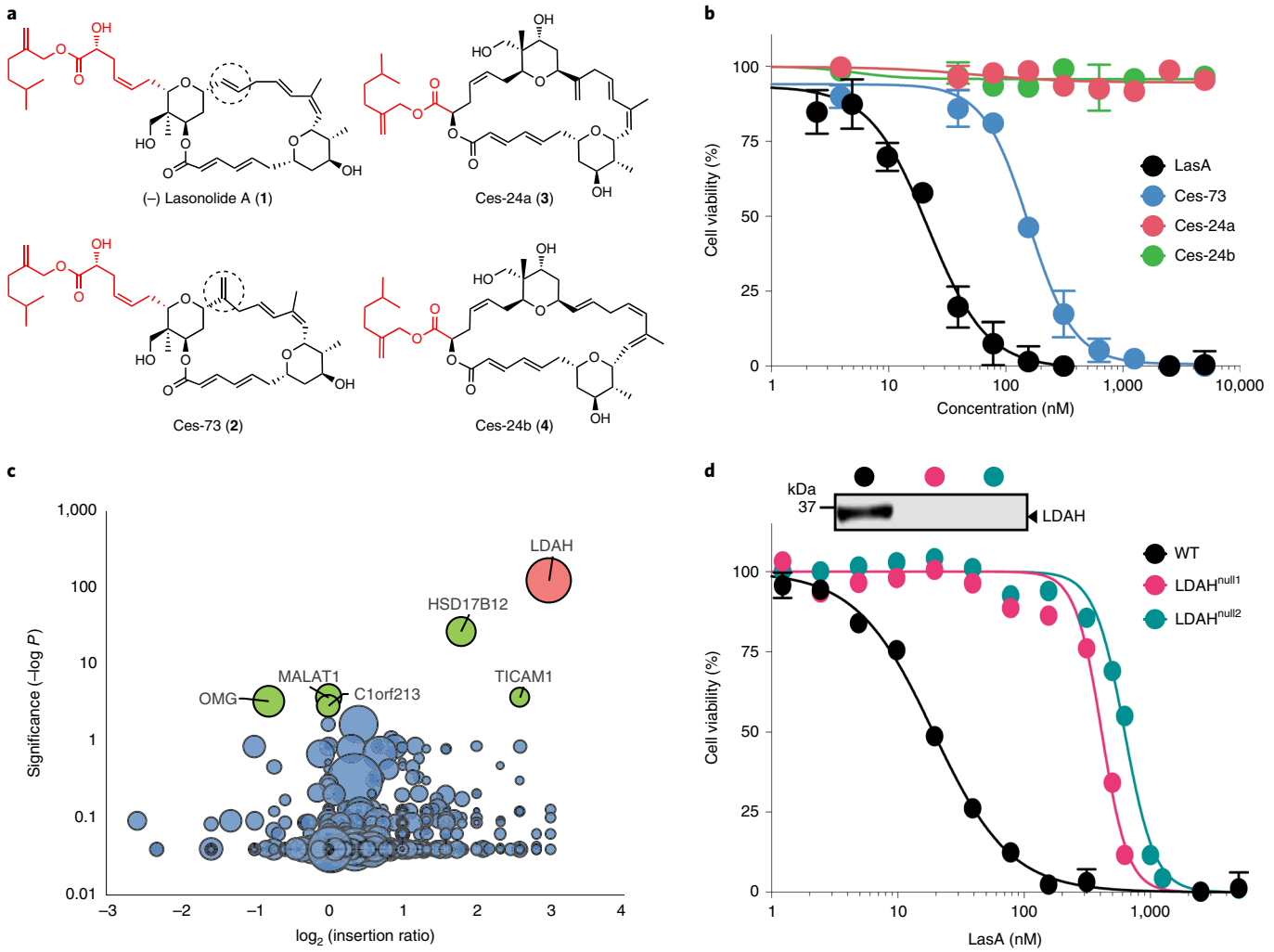

Fig. 1 | Genetic screens in human haploid cells to identify genes required for lasonolide A (LasA) toxicity. a, Structure of (–) lasonolide A and its analogs, with the macrocyclic ring colored in black and the side chain colored in red. Dotted circles highlight the double bond that is endocyclic in LasA but exocyclic in Ces-73. **b**, MTT assays for cell viability were used to determine the IC_{50} values for LasA and its analogs shown in **a**. The IC_{50} values for LasA and Ces-73 are 22 ± 2 nM and 157 ± 11 nM, respectively. **c**, Volcano plot depicting the results of a haploid screen (conducted once, $n = 1$) using cell survival as the selection in the presence of a concentration of LasA that killed >99% of cells. Each circle represents a gene, with the diameter scaled according to the number of independent retroviral insertions, plotted on the basis the *P* value for enrichment of insertions in the drug-selected population over the control population (*y* axis) and the bias toward inactivating intronic insertions (*x* axis). Genes with a false discovery rate-corrected *P* value smaller than 0.01 are colored green, with the exception of the top hit in the screen (LDAH), which is colored pink. The entire dataset for the screen is provided in Supplementary Data 1. *P* values were calculated using the one-sided Fisher exact test and corrected for multiple testing using the Benjamini and Hochberg method. **d**, LasA sensitivity was assessed in $LDAH^{null}$ cell lines using an MTT assay. Immunoblot (representative of three independent repeats) showing abundance of LDAH protein in two clonal cell lines ($LDAH^{null1}$ and $LDAH^{null2}$) carrying CRISPR–Cas9-mediated frameshift mutations in *LDAH* generated using guide RNAs targeting two different exons (Supplementary Fig. 2b with uncropped immunoblot in Supplementary Fig. 10). IC_{50} values for WT, $LDAH^{null1}$ and $LDAH^{null2}$ cell lines were 21 ± 2 nM, 437 ± 17 nM and 636 ± 23 nM, respectively. For panels **b** and **d** the circles denote the mean (±s.d. from $n = 4$ independent samples). Error bars are often smaller than the diameter of the circles used to denote the mean.

LDAH is required for LasA toxicity. We validated the results of the screen by using two independent single guide RNAs (sgRNAs) to introduce inactivating frameshift mutations in *LDAH* (Supplementary Fig. 2b). Both clonal $LDAH^{-/-}$ cell lines showed markedly reduced sensitivity to LasA: the IC_{50} of LasA was >20-fold higher in $LDAH^{-/-}$ Hap1 cells compared to wild-type (WT) Hap1 cells (Fig. 1d). Importantly, the sensitivity to LasA was restored by stable re-expression of LDAH, excluding off-target effects of CRISPR editing (Fig. 2). Increasing the abundance of LDAH protein beyond that seen in wild-type cells did not further increase sensitivity to LasA, suggesting either that other cellular factors become limiting for LasA toxicity above a threshold of LDAH activity or that overexpression of LDAH leads to secondary effects that mitigate toxicity (Supplementary Fig. 3).

We confirmed that the requirement of LDAH for LasA toxicity was not restricted to Hap1 cells. CRISPR-mediated elimination of LDAH protein from MCF7 breast cancer cells, A549 and H1650 lung cancer cells and RKO colon cancer cells also resulted in decreased sensitivity to LasA (Supplementary Fig. 4). Across the NCI-60 panel of cancer cell lines, we found a statistically significant direct correlation between the messenger RNA levels of *LDAH* and sensitivity to LasA[3] (Supplementary Fig. 5).

LDAH belongs to a family of ~117 metabolite serine hydrolases in humans that function as esterases, lipases, peptidases or

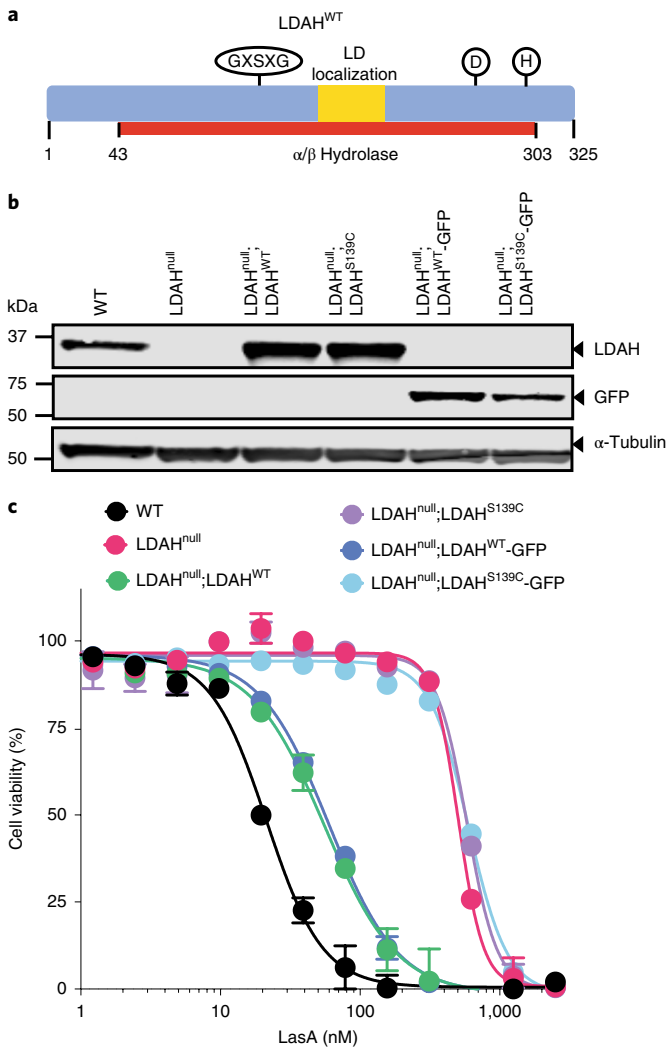

Fig. 2 | The serine hydrolase activity of LDAH is required for LasA toxicity. a, LDAH contains an α/β hydrolase domain (red) with a typical catalytic triad: S139 within a GXSXG motif, D271 and H300 (circled). A hydrophobic hairpin motif that mediates localization to lipid droplets (colored yellow) is present as an insertion in the α/β fold. Numbers refer to amino acid positions. **b**, Abundance of LDAH protein in WT cells, *LDAH*$^{-/-}$ cells (hereafter called LDAH^{null}) and LDAH^{null} cells re-expressing wild-type LDAH (LDAH^{WT}) or a mutant (LDAH^{S139C}) in which the catalytic triad serine (shown in **a**) was changed to cysteine. LDAH^{WT} and LDAH^{S139C} were expressed either as untagged proteins or fused to GFP (uncropped immunoblots are in Supplementary Fig. 10). Immunoblot was repeated three times with similar results. **c**, LasA sensitivity of the indicated cell lines was assessed using an MTT assay. IC_{50} values are as follows: 21 ± 1 nM for WT, 505 ± 22 nM for LDAH^{null}, 56 ± 3 nM for LDAH^{null};LDAH^{WT}, 60 ± 3 nM for LDAH^{null};LDAH^{WT}-GFP, 582 ± 25 nM for LDAH^{null};LDAH^{S139C} and 599 ± 24 nM for LDAH^{null}; hLDAH^{S139C}-GFP. Circles denote the mean value (±s.d. from $n = 3$ independent samples).

amidases[11,12]. Transcriptional profiling by RNA-seq[9] revealed that the mRNA of 99 of these genes was detectable in Hap1 cells (reads per kilobase of transcript, per million (RPKM) > 0), with 74 genes being expressed at RPKM > 1 (ref. [13]) (Supplementary Fig. 6). While mRNA expression does not guarantee protein expression (and protein expression does not guarantee biochemical activity), the broad representation of metabolite serine hydrolases in the Hap1 transcriptome highlights the striking specificity of the requirement of LDAH for LasA sensitivity.

The metabolite serine hydrolases are characterized by an α/β hydrolase fold and a Ser-His-Asp catalytic triad[14–16] (Fig. 2a). While the physiological function of LDAH is unknown, its loss has been linked to an increased risk of prostate cancer[17]. Weak enzymatic activity of LDAH was reported against cholesteroyl esters in vitro, but a *Ldah*$^{-/-}$ mouse was viable and had no defects in cholesterol ester or triacylglycerol metabolism[14,18]. While its endogenous substrate is unknown, LDAH is likely to be enzymatically active because the three catalytic triad residues are conserved in its sequence: a GXSXG motif harboring a putative nucleophilic serine (S139), aspartate (D271) and histidine (H300)[15] (Fig. 2a). To test if the catalytic activity of LDAH was required for its role in sensitizing cells to LasA, we mutated the conserved Ser 139 in LDAH to cysteine (Cys). *LDAH*$^{-/-}$ cells stably expressing LDAH^{S139C} (Fig. 2b) remained resistant to LasA, showing that LDAH catalytic activity was essential for its ability to confer sensitivity to LasA (Fig. 2c). In an important control, the Ser139Cys alteration does not change the abundance of the LDAH protein (Fig. 2b) and also does not change its localization to the surface of lipid droplets[14].

LDAH hydrolyzes LasA to its active metabolite LasF. Why would a serine hydrolase be required for sensitivity of cells to LasA? The fact that *LDAH*$^{-/-}$ cells and *Ldah*$^{-/-}$ mice are viable[18] without any growth defects implies that LasA does not kill cells by blocking LDAH function. Thus, our loss-of-function screens failed to identify the protein target of LasA, perhaps because this target is redundant or required for cell growth or viability. Instead, we considered the possibility that the hydrolytic activity of LDAH may be required for LasA uptake or LasA activation. LasA has two ester bonds, one in the macrocycle and one in the side chain, which could be substrates for a protein with serine hydrolase activity (Fig. 3a). Since cleavage of the ester bond in the macrocyclic ring is likely to destroy activity (based on the structure–activity data presented in Fig.1b), we focused on the ester bond in the side chain (Fig. 3a). Cleavage of this bond would leave a carboxylic acid side chain, which would be charged when unprotonated. In fact, this potential cleavage product was previously isolated from *Forcepia* and named lasonolide F (**5**) (LasF)[2]. We tested the hypothesis that LDAH cleaves LasA into LasF in cells. Since we failed to reconstitute the enzymatic activity of purified LDAH in vitro, we developed a quantitative mass spectrometry assay to measure the levels of the parent LasA and its cleavage product, LasF, in cell extracts (see Methods). In extracts from WT Hap1 cells exposed to LasA, the abundance of cleaved LasF was approximately tenfold higher than LasA (Fig. 3b). Conversely, in Hap1 cell lines lacking LDAH, the ratio was reversed—the parent LasA was tenfold more abundant than its cleavage product LasF (Fig. 3b). The ratio of LasA/LasF, an internally controlled metric that can be compared across cell lines, increased by nearly 100-fold when *LDAH* was disrupted in Hap1 cells (Fig. 3c). Re-expression of wild-type LDAH, but not its catalytically inactive Ser139Cys variant, restored the LasA/LasF ratio to that seen in wild-type cells (Fig. 3b,c). These data show that the enzymatic activity of LDAH is required for the metabolism of LasA into LasF. The total abundance of all lasonolide species (LasA + LasF) did not change much when LDAH was depleted (Fig. 3b), so drug uptake cannot explain the 20-fold greater potency of LasA in WT cells compared to *LDAH*$^{-/-}$ cells.

These results support the hypothesis that LDAH is required for cell sensitivity to LasA because it converts the prodrug LasA into the active drug LasF, the molecule that kills cells rather than LasA itself. The logarithm of the octanol/water partition coefficient of a drug (called the log *P*) is commonly used to evaluate the suitability of small molecules to permeate cell membranes. The predicted log *P* of LasA is 5.98, while the log *P* of the deprotonated, charged form of LasF is predicted to be much lower at −0.55 (the log *P* of the protonated form would be ~2.29). The high hydrophobicity of LasA implies that it would readily partition into the plasma membrane

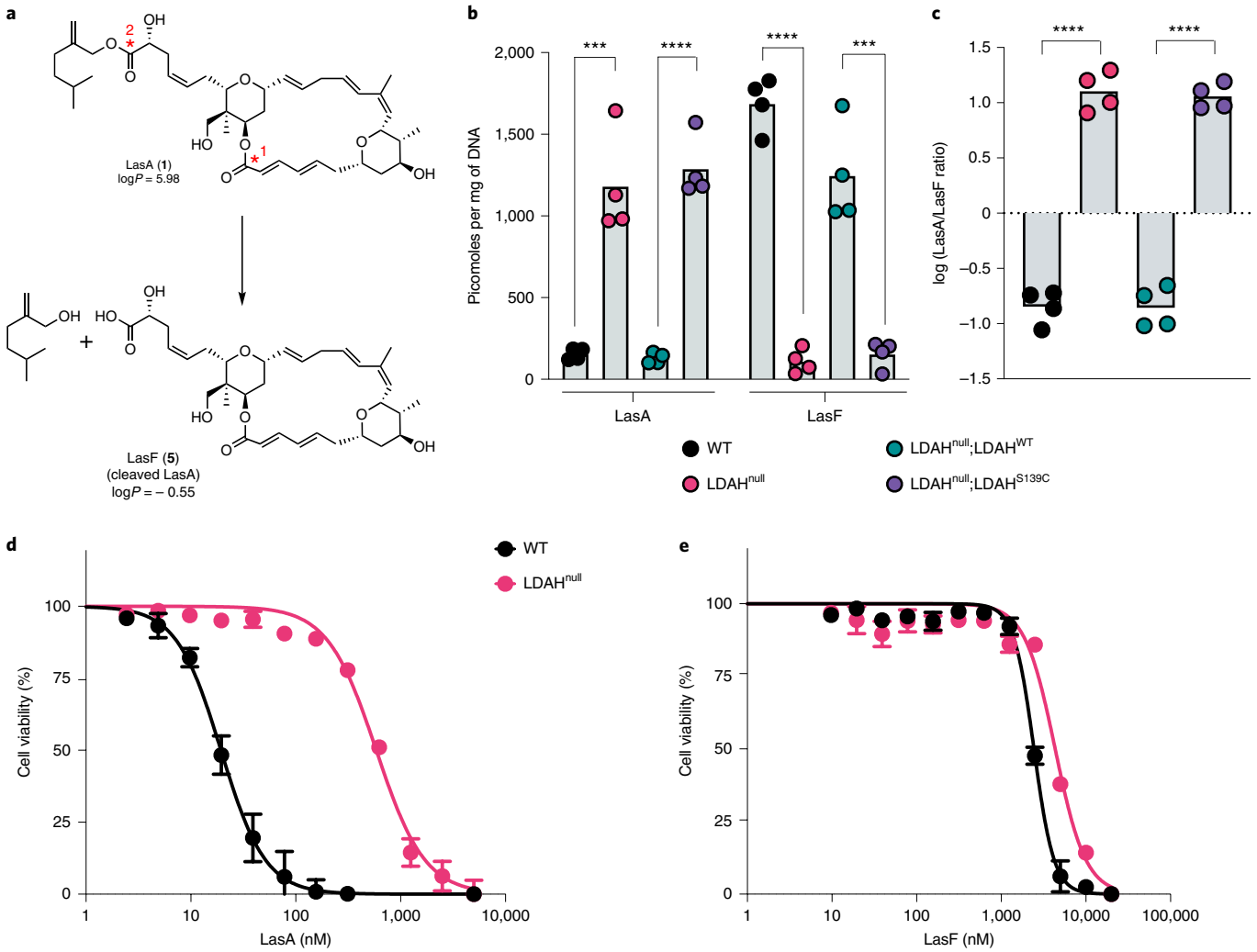

Fig. 3 | LDAH converts LasA to LasF by cleaving its side chain. a, LDAH may catalyze the hydrolysis of LasA to LasF by cleaving the ester bond (marked 2) in the side chain. **b**, The abundances of LasA and LasF, normalized using the genomic DNA content in each sample, were measured by quantitative mass spectrometry (see Methods). **c**, The ratio of the abundance of LasA to LasF for each independent experiment is depicted (on a logarithmic scale) for the four indicated cell lines. **d**,**e**, Sensitivity to LasA and LasF in wild-type (WT) and LDAH^{null} cells was assessed using an MTT assay. IC_{50} values for LasA (**d**) in WT and LDAH^{null} cell lines are 19 ± 1 nM and 586 ± 34 nM, respectively, and for LasF (**e**) are 2.4 ± 0.1 μM and 4.3 ± 0.4 μM, respectively. Circles denote the mean value (±s.d. from $n = 3$ independent samples). Significance in **b** and **c** was tested using a two-tailed, unpaired *t*-test and is indicated as ***$P < 0.001$ or **$P < 0.01$. The circles in **b** and **c** denote data from four different experiments in each of the indicated cell lines.

but would likely accumulate in the membrane and other lipophilic compartments rather than crossing into the cytoplasm. In contrast, the charged form of LasF may have difficulty partitioning into the plasma membrane and hence in permeating into cells. Indeed, LasF, when directly applied to Hap1 cells, was much less potent than LasA (Fig. 3d,e), a result consistent with published data from cancer cell lines[2]. Importantly, the IC_{50} of LasF was minimally affected by the depletion of LDAH, supporting the model that the function of LDAH is to convert LasA to LasF (Fig. 3d,e).

LasA toxicity requires membrane-localized LDAH. To understand how LDAH may gain access to the hydrophobic LasA for cleavage, we first looked at the subcellular localization of green fluorescent protein (GFP)-tagged LDAH. LDAH-GFP was functional because it could restore LasA toxicity to *LDAH*$^{-/-}$ cells (Fig. 2b,c). As reported previously[15], LDAH was found localized on the surface of lipid droplets and in the endoplasmic reticulum (ER) (Fig. 4a, Supplementary Fig. 7 and Supplementary Video 1). Like some (class I) lipid droplet proteins, LDAH is thought to move from the ER to the surface of lipid droplets as they emerge from the cytoplasmic leaflet of the ER[15,19]. These observations suggested the possibility that LasA activation by cleavage to LasF occurs at a membrane interface—either at the ER membrane or at the surface of lipid droplets. To test the idea that membrane localization of LDAH was required for its ability to activate LasA, we took advantage of the previous observation that LDAH inserts into the phospholipid monolayer surface of lipid droplets using a hydrophobic hairpin motif (Fig. 4b)[15,18]. Two different truncating mutations that removed portions of this motif eliminated LDAH localization to lipid droplets while maintaining LDAH protein expression (Fig. 4c,d). Both mutations completely eliminated the ability of LDAH to sensitize cells to LasA (Fig. 4e), suggesting that localization of the enzyme to membranes was required for its ability to cleave LasA to LasF.

Lipid droplets promote the toxicity of LasA. We next tested the concept that lipid droplets play a role in the activation of LasA by LDAH. First, we used established manipulations to increase or

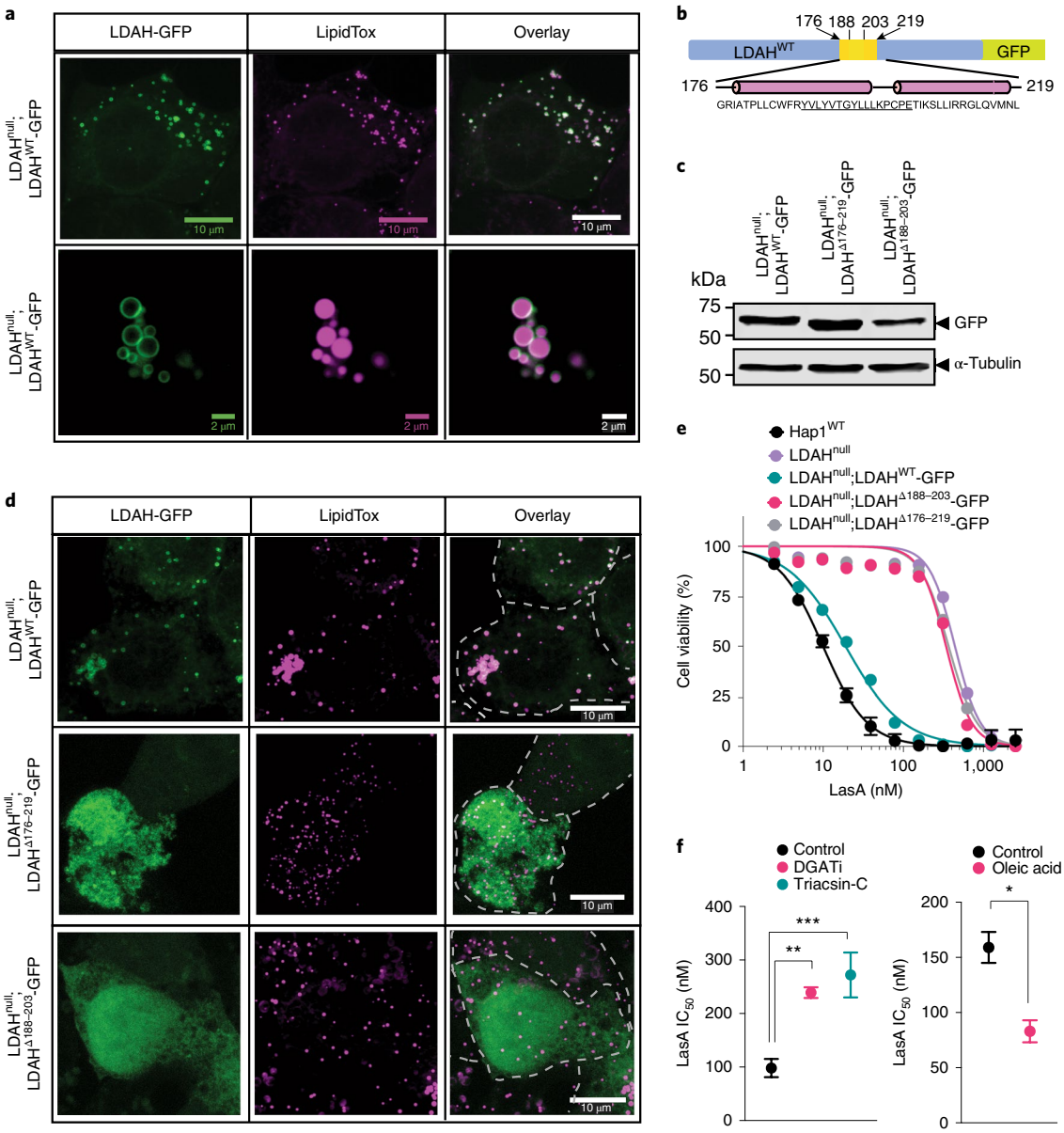

Fig. 4 | Membrane localization of LDAH is required for LasA sensitivity. a, LDAH-GFP (green) is localized on the surface of lipid droplets, marked by the LipidTox stain (red). Images at two different magnifications are shown in the top (scale bar, 10 μm) and bottom panels (scale bar, 2 μm). Localization in live cells is shown in Supplementary Fig. 7. The experiment was repeated three times with similar results. **b**–**d**, The hydrophobic hairpin motif (yellow) in LDAH-GFP was interrupted by replacing two regions (LDAH176–219 or the shorter LDAH188–203) with a flexible linker sequence (**b**). These LDAH-GFP mutant proteins were stably expressed in LDAH^{null} cells and their abundances were assessed by immunoblotting (**c**) and their localization to lipid droplets was assessed by immunofluorescence (**d**, scale bar 10 μm). Experiments were repeated three times with similar results. Uncropped immunoblots are in Supplementary Fig. 10. **e**, LasA sensitivity was measured in the indicated cell lines by an MTT assay. IC_{50} values are as follows: 440 ± 32 nM for LDAH^{null}, 10 ± 1 nM for Hap1^{WT}, 19 ± 1 nM for LDAH^{null};LDAH^{WT}-GFP, 367 ± 26 nM for LDAH^{null};LDAH$^{Δ176-219}$-GFP, 341 ± 29 nM for LDAH^{null};LDAH$^{Δ188-203}$-GFP. Circles denote the mean (±s.d. from $n = 4$ independent samples). **f**, The IC_{50} values of LasA, measured by the MTT assay, in cells exposed to DGAT inhibitors (20 μM T863 and 10 μM PF-06424439), Triacsin-C (1 μM) or oleic acid (200 μM, right graph). Circles denote mean IC_{50} (from $n = 3$ independent samples) and error bars denote the standard error of the curve fit used to calculate the IC_{50}. Significance in **f** was determined by a two-tailed, unpaired *t*-test and is indicated as $^{**}P < 0.01$ or $^{*}P < 0.05$.

decrease lipid droplet number in cells. Oleic acid was used to enhance the lipid droplet content of cells, while treatment with diacylglycerol *O*-acyltransferase (DGAT) inhibitors (T863 and PF-06424439) or a long chain fatty acid acyl-CoA synthetase inhibitor (triacsin-C) decreased the lipid droplet content of cells (Supplementary Fig. 8). The IC_{50} of LasA correlated with cellular lipid droplet content—increasing the number of lipid droplets with oleic acid increased the potency of the drug, while decreasing the lipid droplet content by inhibiting triglyceride and cholesterol ester synthesis reduced the potency of the drug by 2–3-fold (Fig. 4f).

We also analyzed the subcellular distribution of LasA and LasF by cell fractionation. Postnuclear supernatants (PNS) derived from LasA-treated cells were separated by discontinuous density gradient centrifugation into three fractions[20]: lipid droplets, which float due to their uniquely lower density in comparison to other cellular compartments, cytoplasm and cellular membranes, including the

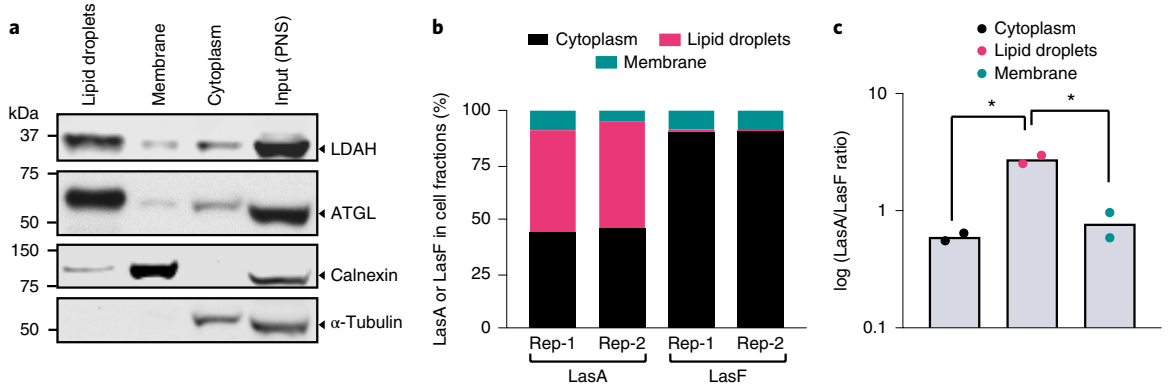

Fig. 5 | Subcellular distribution of LasA and LasF. a, An equal proportion of each subcellular fraction (see Supplementary Fig. 9) was used to assess the abundance of LDAH and established protein markers of the cytoplasm (α-tubulin), ER (calnexin) or lipid droplets (ATGL) by immunoblotting (uncropped immunoblots are in Supplementary Fig. 11). The experiment was repeated twice with similar results. **b**, The distribution of total LasA and LasF in each of the three fractions as measured by quantitative mass spectrometry. Rep-1 and Rep-2 show results from two different experiments. **c**, The ratio of the abundance of LasA to LasF in the lipid droplet, cytoplasm and membrane fraction is shown on a logarithmic scale. Each dot represents a different experiment ($n = 2$). Significance in **c** was determined by a two-tailed, unpaired t-test and is indicated by $^*P < 0.05$.

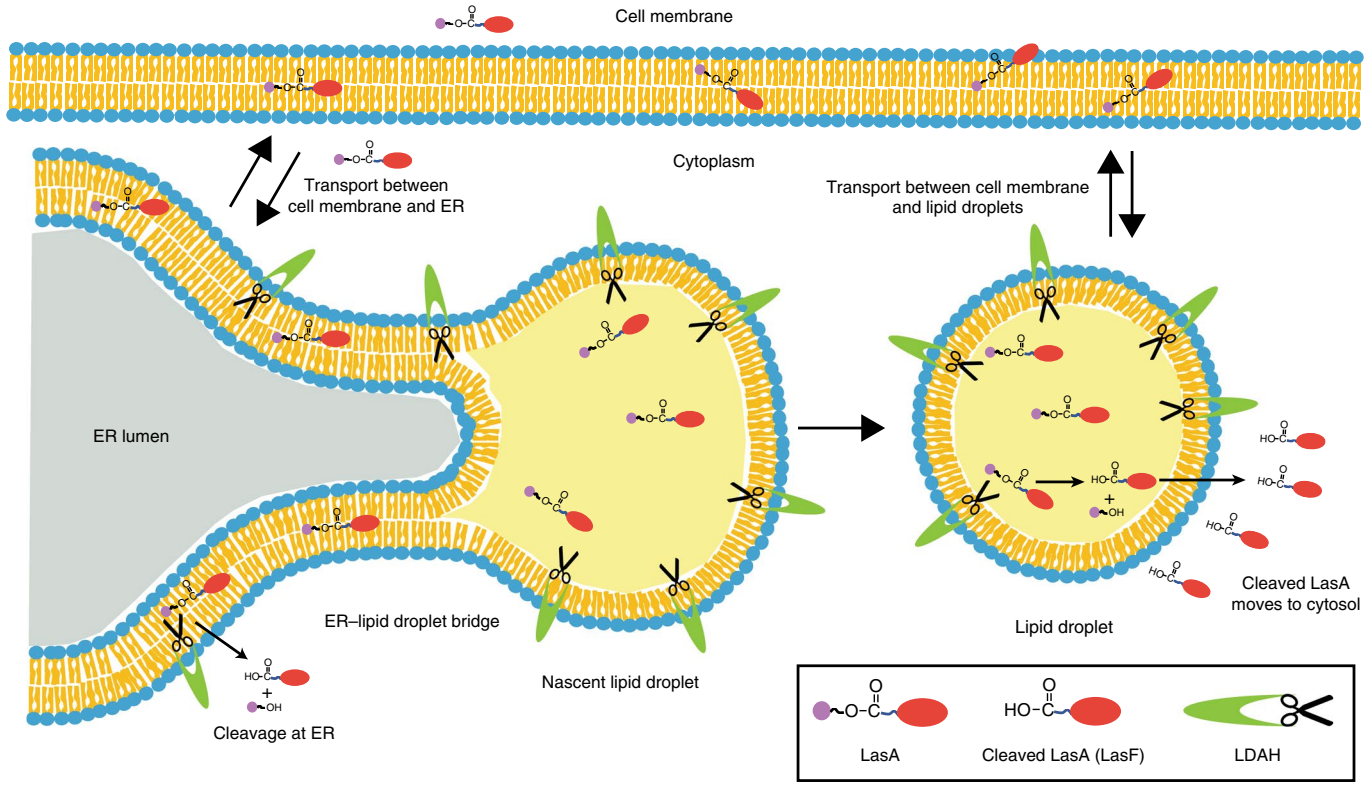

Fig. 6 | A proposed mechanism for the uptake of LasA and its activation by LDAH-mediated cleavage. LasA traverses the plasma membrane and accumulates in lipid droplets, likely by selective partitioning into its oil-like core (light yellow). LDAH is also found in the ER, but it accumulates to the highest levels on the surface of lipid droplets proximal to the reservoir of LasA in the lipid droplet core. LDAH can likely cleave LasA to LasF either at the ER or lipid droplet surface.

ER (Supplementary Fig. 9). The quality of the fractionation was established by immunoblotting using antibodies against markers for each compartment (Fig. 5a): ATGL, a commonly used marker of lipid droplets, and LDAH were predominantly found in the lipid droplet fraction, while calnexin, an ER marker, was found in the membrane fraction. LasA and LasF were measured in each fraction using our mass spectrometry assay (Fig. 3). LasA was equally distributed between the cytoplasm and the lipid droplet fraction, while LasF was mostly found in the cytoplasm (Fig. 5b). The abundances of both LasA and LasF were similar in the membrane fractions. As a result, the LasA/LasF ratio is highest in the lipid droplets and lowest in the cytoplasm (Fig. 5c). Thus, amongst membrane-bound compartments in cells, LasA showed a striking propensity to accumulate in lipid droplets.

Discussion

Our results uncovered an unexpected cellular route for the activation of the potent cytotoxic macrolide LasA (depicted in Fig. 6).

We propose that LasA partitions into the plasma membrane and then gains access to lipid droplets, either directly or via the membrane of the ER, since the phospholipid monolayer that invests lipid droplets is derived from the cytoplasmic leaflet of the ER. How LasA moves from the plasma membrane, the first barrier for any drug, to the ER or to lipid droplets remains unknown but we speculate that this may occur at interorganelle contact sites. Importantly, LasA seems to preferentially accumulate in lipid droplets over other membrane compartments (Fig. 5b) while LasF, the cleavage product of LasA and likely the active metabolite, was mostly localized in the cytoplasm. Given the highly hydrophobic nature of LasA (calculated log *P* of ~6), the presence of LasA in the cytoplasm (Fig. 5b) was unexpected, although we cannot exclude artifacts caused by organelle damage and consequent drug leakage during the inherently disruptive process of cell fractionation. Alternatively, LasA may bind to cytoplasmic proteins that shuttle it to lipid droplets. The mechanism for why LasA accumulates in lipid droplets is unknown, but its highly hydrophobic nature may favor selective partitioning into the oil-like hydrophobic core composed of neutral lipids, such as triglycerides and cholesterol esters. Cleavage of LasA to the more polar LasF (Fig. 3a) would undoubtedly reduce its propensity to partition in the oil-phase core of lipid droplets and hence promote its release into the cytoplasm.

The accumulation of both LasA and LDAH in lipid droplets (Figs. 4a and 5b) may accelerate the LasA to LasF cleavage reaction by concentrating the enzyme and its substrate in close proximity. This property of concentrating reactants by selective partitioning is emerging as one of the key biochemical functions of phase-separated compartments in cells[14,21]. More generally, lipid droplets and other phase-separated organelles may function as reservoirs for drug-like small molecules in cells. For example, a recent study found that the accumulation of a lipophilic antibiotic (bedaquiline) in lipid droplets enhances its antibacterial action against *Mycobacterium tuberculosis*[22]. In both our studies on LasA and the published work on bedaquiline, lipid droplets contribute to drug efficacy but are not absolutely required: the IC_{50} of LasA is reduced by 2–3-fold by treatments that deplete lipid droplets (Fig. 4f) but by ~20-fold when LDAH is ablated (Fig. 1d). Thus, LDAH is likely capable of converting LasA to LasF even in the absence of lipid droplets. Since membrane localization of LDAH is required for cell sensitivity to LasA (Fig. 4e), it may also be able to activate LasA at the surface of the ER. More generally, our work shows that the subcellular localization or accumulation of drugs can influence their efficacies. A challenge that must be overcome is to develop better analytic methods, such as ion microscopy or imaging mass spectrometry, to assess the distribution of small molecules in cells at subcellular or even suborganelle resolution[22,23].

Lipid droplets are dynamic organelles that accumulate in diverse pathological states, especially those linked to inflammatory stress[24]. Activated myeloid cells, such as the 'foamy' macrophages seen in atherosclerotic lesions, are characterized by large numbers of lipid droplets[25]. Indeed, this may be the reason that bedaquiline is particularly effective against mycobacteria that have infected macrophages[22]. For over a century, pathological lesions of Alzheimer's disease have also been noted to contain high levels of lipid droplets[26]. Lipid droplets are increased in several types of cancer cells[27,28], including clear cell renal cancer[29], prostate cancer[30] and breast cancer[31], and this increase has been correlated with tumor aggressiveness[32]. Nutrient deprivation, hypoxia and chemotherapy exposure, in addition to inflammatory stress, have been postulated to promote lipid droplet biogenesis in cancer cells. Cancer types with increased lipid droplet number may be particularly vulnerable to drugs like LasA that exploit a lipid droplet-based mechanism of toxicity. Medicinal chemistry strategies to modify small molecules to drive their accumulation in lipid droplets, or to take advantage of the enzymes found in lipid droplets, could allow this approach to be applied to other small-molecule therapeutics for cancer, inflammation and neurodegeneration.

The use of alkyl esters to make prodrugs with improved cell permeability is a well-established strategy: nearly one-third of the approved prodrugs in the last decade utilize cleavage of an ester bond for drug activation[33]. In most cases, these esterified prodrugs are activated promiscuously by the many esterases present in cells. In contrast, the cleavage of LasA is not a generic ester hydrolysis reaction, but instead is highly selective in its requirement for LDAH. This selectivity suggests that it may be possible to achieve tissue or tumor selectivity in prodrug design by matching the prodrug and structure of the ester side chain to the substrate specificity of a hydrolase expressed specifically in the target tissue. In summary, our work highlights the power of genetic screens to provide actionable insights, not just into drug targets, but also into the mechanisms of drug uptake and activation.

Online content

Any methods, additional references, Nature Research reporting summaries, source data, extended data, supplementary information, acknowledgements, peer review information; details of author contributions and competing interests; and statements of data and code availability are available at https://doi.org/10.1038/s41589-019-0447-7.

Received: 13 February 2019; Accepted: 2 December 2019;
Published online: 13 January 2020

References

1. Horton, P. A., Koehn, F. E., Longley, R. E. & McConnell, O. J. Lasonolide A, a new cytotoxic macrolide from the marine sponge *Forcepia* sp. *J. Am. Chem. Soc.* **116**, 6015–6016 (1994).
2. Wright, A. E. et al. Lasonolides C–G, five new lasonolide compounds from the sponge *Forcepia* sp. *J. Nat. Prod.* **67**, 1351–1355 (2004).
3. Isbrucker, R. A., Guzman, E. A., Pitts, T. P. & Wright, A. E. Early effects of lasonolide A on pancreatic cancer cells. *J. Pharmacol. Exp. Ther.* **331**, 733–739 (2009).
4. Zhang, Y. W., Ghosh, A. K. & Pommier, Y. Lasonolide A, a potent and reversible inducer of chromosome condensation. *Cell Cycle* **11**, 4424–4435 (2012).
5. Josse, R. et al. Activation of RAF1 (c-RAF) by the marine alkaloid lasonolide A induces rapid premature chromosome condensation. *Mar. Drugs* **13**, 3625–3639 (2015).
6. Trost, B. M. et al. Total synthesis of (−)-lasonolide A. *J. Am. Chem. Soc.* **138**, 11690–11701 (2016).
7. Carette, J. E. et al. Haploid genetic screens in human cells identify host factors used by pathogens. *Science* **326**, 1231–1235 (2009).
8. Carette, J. E. et al. Global gene disruption in human cells to assign genes to phenotypes by deep sequencing. *Nat. Biotechnol.* **29**, 542–546 (2011).
9. Dubey, R. et al. Chromatin-remodeling complex SWI/SNF controls multidrug resistance by transcriptionally regulating the drug efflux pump ABCB1. *Cancer Res.* **76**, 5810–5821 (2016).
10. Carette, J. E. et al. Ebola virus entry requires the cholesterol transporter Niemann–Pick C1. *Nature* **477**, 340–343 (2011).
11. Simon, G. M. & Cravatt, B. F. Activity-based proteomics of enzyme superfamilies: serine hydrolases as a case study. *J. Biol. Chem.* **285**, 11051–11055 (2010).
12. Bachovchin, D. A. & Cravatt, B. F. The pharmacological landscape and therapeutic potential of serine hydrolases. *Nat. Rev. Drug Discov.* **11**, 52–68 (2012).
13. Hebenstreit, D. et al. RNA sequencing reveals two major classes of gene expression levels in metazoan cells. *Mol. Syst. Biol.* **7**, 497–497 (2011).
14. Goo, Y. H., Son, S. H., Kreienberg, P. B. & Paul, A. Novel lipid droplet-associated serine hydrolase regulates macrophage cholesterol mobilization. *Arterioscler. Thromb. Vasc. Biol.* **34**, 386–396 (2014).
15. Thiel, K. et al. The evolutionarily conserved protein CG9186 is associated with lipid droplets, required for their positioning and for fat storage. *J. Cell Sci.* **126**, 2198–2212 (2013).
16. Marchler-Bauer, A. et al. CDD: NCBI's conserved domain database. *Nucleic Acids Res.* **43**, D222–D226 (2015).
17. Currall, B. B. et al. Loss of LDAH associated with prostate cancer and hearing loss. *Hum. Mol. Genet.* **27**, 4194–4203 (2018).

18. Kory, N. et al. Mice lacking lipid droplet-associated hydrolase, a gene linked to human prostate cancer, have normal cholesterol ester metabolism. *J. Lipid Res.* **58**, 226–235 (2017).
19. Olzmann, J. A. & Carvalho, P. Dynamics and functions of lipid droplets. *Nat. Rev. Mol. Cell Biol.* **20**, 137–155 (2019).
20. Brasaemle, D. L. & Wolins, N. E. Isolation of lipid droplets from cells by density gradient centrifugation. *Curr. Protoc. Cell Biol.* **72**, 3.15. 1–3.15.13 (2016).
21. Banani, S. F., Lee, H. O., Hyman, A. A. & Rosen, M. K. Biomolecular condensates: organizers of cellular biochemistry. *Nat. Rev. Mol. Cell Biol.* **18**, 285–298 (2017).
22. Greenwood, D. J. et al. Subcellular antibiotic visualization reveals a dynamic drug reservoir in infected macrophages. *Science* **364**, 1279–1282 (2019).
23. Zheng, N., Tsai, H. N., Zhang, X. & Rosania, G. R. The subcellular distribution of small molecules: from pharmacokinetics to synthetic biology. *Mol. Pharm.* **8**, 1619–1628 (2011).
24. den Brok, M. H., Raaijmakers, T. K., Collado-Camps, E. & Adema, G. J. Lipid droplets as immune modulators in myeloid cells. *Trends Immunol.* **39**, 380–392 (2018).
25. Fowler, S., Shio, H. & Haley, N. J. Characterization of lipid-laden aortic cells from cholesterol-fed rabbits. IV. Investigation of macrophage-like properties of aortic cell populations. *Lab. Investig.* **41**, 372–378 (1979).
26. Foley, P. Lipids in Alzheimer's disease: a century-old story. *Biochim. Biophys. Acta* **1801**, 750–753 (2010).
27. Delikatny, E. J., Chawla, S., Leung, D.-J. & Poptani, H. MR-visible lipids and the tumor microenvironment. *NMR Biomedicine* **24**, 592–611 (2011).
28. Petan, T., Jarc, E. & Jusović, M. Lipid droplets in cancer: guardians of fat in a stressful world. *Molecules* **23**, 1941 (2018).
29. Sundelin, J. P. et al. Increased expression of the very low-density lipoprotein receptor mediates lipid accumulation in clear-cell renal cell carcinoma. *PLoS ONE* **7**, e48694 (2012).
30. Hager, M. H., Solomon, K. R. & Freeman, M. R. The role of cholesterol in prostate cancer. *Curr. Opin. Clin. Nutr. Metab. Care* **9**, 379–385 (2006).
31. Aboumrad, M. H., Horn, R. C. Jr. & Fine, G. Lipid-secreting mammary carcinoma. Report of a case associated with Paget's disease of the nipple. *Cancer* **16**, 521–525 (1963).
32. Ramos, C. V. & Taylor, H. B. Lipid-rich carcinoma of the breast. A clinicopathologic analysis of 13 examples. *Cancer* **33**, 812–819 (1974).
33. Rautio, J., Meanwell, N. A., Di, L. & Hageman, M. J. The expanding role of prodrugs in contemporary drug design and development. *Nat. Rev. Drug Discov.* **17**, 559–587 (2018).

Methods

Cell lines. The Hap1 cell line[10] was kindly provided by T. Brummelkamp, Netherlands Cancer Institute, and validated by confirming its haploid genomic DNA content at regular intervals during the screens. The 293FT cell line used to generate high-titer lentiviruses was obtained from ThermoFisher Scientific; the MCF7, H1650, A549 and RKO cell lines were purchased from American Type Culture Collection. Purchased cell lines came with a certificate of authenticity. We did not further validate cell lines but used them at passages <10. All cell lines were confirmed to be negative for *Mycoplasma* contamination. Hap1 cells were grown in IMDM with 10% FBS and 6 mM L-glutamine; 293FT in DMEM with 10% FBS, 1 mM sodium pyruvate, 1× MEM-NEAA and 2 mM L-glutamine; MCF7 cells in RPMI with 10% FBS and 2 mM L-glutamine.

Constructs and alleles. Null alleles for LDAH were constructed using the CRISPR–Cas9 system. For Hap1 cells the oligonucleotides encoding the guide RNAs were cloned into pSpCas9(BB)-2A-GFP (PX458, Addgene plasmid no. 48138) kindly provided by F. Zhang[34]. The sequences for target sites for the two sgRNAs were guide1: GACCTACTTACCGGGAGCTC and guide2: GTAGCTAATGCTGCCTACCT. Single cells were sorted using flow cytometry, expanded and clones bearing null alleles were identified by Sanger sequencing and immunoblotting. For gene disruption MCF7 cells, the following four guide RNAs targeting LDAH were introduced into LentiCRISPR v.2 (Addgene plasmid no. 52961), kindly provided by F. Zhang[35] for lentiviral-mediated delivery. Lenti-CR1: CAAGTCCTTGCTAATCAGAA, Lenti-CR2: CCTGAGAACTCATGTGCCAA, Lenti-CR3: CGAATGTCTGAGTCACCCAA, Lenti-CR4: GAAGATTCTTACAACATCAG. For gene disruption in H1650, A549 and RKO cell lines, Lenti-CR2 was used.

LDAH constructs were based on the human LDAH gene purchased from GeneCopoeia[14]. LDAH-GFP fusion constructs were created using Gibson assembly and S139C mutants were made using site-directed mutagenesis (Quickchange). LDAH mutants lacking the lipid droplet localizing hairpin motifs (Fig. 4b) were made using Gibson assembly where the residues from 176–219 or 188–203 were replaced with a linker sequence 'SSSGGGGSGGGGS'. Mutants were subcloned into pLenti-CMV-Puro-DEST[36] (plasmid no. 17452) from Addgene kindly provided by E. Campeau for stable expression. Lentivirus (generated in 293FT)-infected cells were selected with 2 μg ml^{-1} of puromycin for 2 weeks.

Chemical compounds. Synthesis and characterization of LasA, Ces-73, Ces-24a and Ces-24b have been described previously[6,37]. LasA, Ces-73, Ces-24a and Ces-24b are annotated as (−)-lasonolide A, compounds 106, 105 and 104 (respectively) in these previous papers. ChemDraw Professional v.16 was used to calculate log *P* values of LasA and LasF. T863 (≥98%), PF-06424439 (≥98%) and triacsin-C (≥98%) were purchased from Millipore Sigma.

To generate LasF from LasA at microscale, tetrakis(triphenylphosphine) palladium(0) (1.0 equiv.) was added to a solution of lasonolide A (LasA) (0.1 mg, 0.14 μM) and morpholine (10.0 equiv.) in tetrahydrofuran (0.5 ml) at room temperature. After 30 min, the reaction was concentrated under a stream of nitrogen. The liquid chromatography–mass spectrometry (LC–MS) of the residue confirmed full conversion of LasA into LasF (LasF ~98.3% pure) and this material was used in subsequent experiments without further purification. High-resolution MS (HRMS): (ESI) calcd for $C_{33}H_{47}O_9$ $[M+H]^+$ 587.3220; found 587.3332.

Haploid genetic screens. Methods for the execution of haploid genetic screens using insertional retroviral mutagenesis and the bioinformatic pipeline to map the distribution of these insertions in the genome have been described previously[8,9]. One hundred million mutagenized Hap1 cells were treated with LasA (80 nM) or Ces-73 (400 nM) for a total of 8 d, replenishing the media after the first 2 d only with fresh LasA or Ces-73. Surviving cells were allowed to recover and expand for 1 week in the absence of LasA or Ces-73 before collection. Genome-wide mapping of insertions was performed in a pool of 30 million LasA/Ces-73-resistant cells and compared to insertions mapped in an equal number of cells from the mutant library before drug selection. Results of the screen were analyzed as detailed previously[9,10] and the computational pipeline is available on github: https://github.com/RohatgiLab/BAIMS-Pipeline.

Cytotoxicity assays. A total of 20,000 cells were plated in each well of a 96-well plate, allowed to grow for 24 h and then treated with various concentrations of LasA, Ces-24a, Ces-24b, Ces-73 or LasF in replicates; the concentration of the solvent (DMSO) in which these compounds were dissolved was normalized across all wells to 0.1% (v/v). Assays were performed after either short-term drug exposure (30 min), to measure the known immediate effects on LasA on cell attachment, or after long-term drug exposure (45 h) to measure viability. After washing plates to remove unattached or dead cells, the assay was performed by adding 10 μl of 5 mg ml^{-1} MTT (3-(4,5-dimethylthiazol-2-yl)-2, 5-diphenyltetrazolium bromide) reagent to each well. Cells were incubated for 3 h with the MTT reagent, media was removed and 50 μl of DMSO was added to each well to solubilize the purple-colored formazan. Absorbance was read at 570 nm on a Biotek Synergy HT microplate reader.

For inhibitor studies, cells were treated with a combination of T863 (20 μM) and PF-06424439 (10 μM), triacsin-C alone (1 μM) or oleic acid (200 μM) for 24 h before exposure to LasA. For oleic acid treatment, 20 μl of a 200-mM stock of oleic acid in ethanol was first added to 2 ml of 10% BSA (w/v) and incubated at 37 °C for 30 min until the solution cleared. This mixture was added to 18 ml of normal growth medium to achieve an oleic acid concentration of 200 μM and a BSA fraction of 1% (w/v).

Immunoblotting. Cells were scraped into ice-cold PBS containing 1× SigmaFast Protease Inhibitor Cocktail (Roche) and collected as a pellet by centrifugation (500*g*, 5 min, 4 °C). Cells were lysed (45 min, 4 °C) by agitation in modified RIPA buffer (50 mM Tris–HCl, pH 8.0, 150 mM NaCl, 2% NP-40, 0.25% deoxycholate, 0.1% SDS, 1 mM NaF, 1 mM DTT, 1× SigmaFast, 10% glycerol), followed by centrifugation at 20,000*g* for 30 min at 4 °C and determination of the total protein concentration in each lysate using the Pierce BCA Protein Assay Kit (ThermoFisher Scientific). Equal amounts of each lysate (50 μg) were fractionated by 8% PAGE, transferred to nitrocellulose membrane and blocked with 0.1% casein in 0.2× PBS for 1 h at room temperature. Membranes were incubated with protein-specific antibodies overnight at 4 °C followed by 1-h treatment with secondary antibodies, before quantification using chemiluminescence or LiCOR Odyssey. Antibodies used were as follows: anti-LDAH (described previously[14]); anti-GFP (NB600-308) from Novus Biologicals; anti-calnexin (ADI-SPA-865-D) from Enzo Life Sciences; anti-ATGL (2138S) from Cell Signaling Technology; anti-α-tubulin (T6199) from Sigma-Aldrich.

Measurement of LasA and LasF in cell extracts by quantitative mass spectrometry. *Sample preparation.* Cells expressing LDAH variants grown in 15-cm culture plates to ~80% confluency were treated with 200 nM LasA for 1 h and washed with cold PBS. Cells from each 15-cm plate were scraped into 5 ml of a methanol/chloroform (9:1) mixture in the cold room, transferred to a 15-ml tube, mixed by thorough pipetting and centrifuged at 2,000*g* to remove insoluble debris. The supernatant was transferred to a 20-ml scintillation vial and concentrated under vacuum to remove the methanol/chloroform mixture. The samples were stored at −80 °C before analysis by LC–MS.

Subcellular fractionation studies (Fig. 5) were performed with cells grown in three 15-cm plates and treated with 200 μM oleic acid for 24 h followed by LasA (200 nM) for 1 h before collection. Cells were washed with ice-cold PBS and collected by scraping in 1 ml of PBS per 15-cm plate into a 15-ml tube. The cells were pelleted by centrifugation and resuspended at 4 °C in hypotonic lysis medium (HLM) buffer (20 mM Tris, pH 7.4, 1 mM EDTA, 10 mM NaF) for 15 min. The cells were lysed by subjecting them to 20 strokes in a Dounce homogenizer using a tight pestle, followed by two cycles of centrifugation (1,000*g* for 10 min) to pellet the nuclei and large debris. The resultant PNS was brought to 20% sucrose (w/w) by supplementing from 60% (w/w) sucrose stock and then layered at the bottom of an ultracentrifuge tube (Beckman, Ultra-clear 16 mm × 102 mm). The PNS (2.5 ml in 20% sucrose) was overlaid sequentially with 3 ml of 5% sucrose in HLM and finally with HLM solution lacking any sucrose (Supplementary Fig. 9). After centrifugation in (SW28 rotor) at 120,000*g* for 1 h at 4 °C, the lipid droplet layer on the top of the gradient was removed with a tube slicer (Beckman). The remaining solution in the tube was taken as the cytoplasm and the membrane-containing pellet was collected separately in 2 ml of HLM (Fig. 5a). The entirety of the three cell fractions (lipid droplet, membrane and cytoplasm) was extracted using a chloroform/ethyl acetate (1:1) mixture and the organic phase was transferred to a 20-ml scintillation vial for solvent removal under vacuum. Samples were stored at −80 °C before analysis by LC–MS.

To fully recover the samples before mass spectrometry, each scintillation vial was washed down with 1 ml of methanol, sonicated for 1 min, transferred to an eppendorf vial and evaporated to dryness. All standards and samples were reconstituted in 150 μl of methanol and transferred to autosampler vials.

Liquid chromatography and mass spectrometry. Samples were analyzed using a 1290 Infinity II UPLC integrated with a 6560 IM-QTOF (Agilent Technologies). Liquid chromatography was performed on a 2.1 mm × 50 mm Acquity UPLC BEH C18 column (1.7 μm particle size) with gradient elution at a flow rate of 0.50 ml min^{-1} and temperature of 35 °C. Mobile phases were 50 mM NH_4Ac in water (A) and 0.1% formic acid in acetonitrile (B). Gradient elution profile: initial hold at 35% B for 2 min, followed by a linear gradient of 35%–95% B in 3 min, then hold at 95% B for 1 min before equilibrating back to 35% B; total run time was 7 min. The mass spectrometer acquired full scan (m/z 100–1,700) using dual AJS ESI source in negative mode. While LasA and LasF ionize in both positive and negative modes, higher ionization efficiency was achieved in negative mode. Measurements were done at MS1 level (full mass scan). To maximize the LC–MS method sensitivity, LasA (HAc adduct, $M+HAc-H$; $m/z=755.01$) and LasF ($M-H$; $m/z=585.3$) were monitored using targeted EIC channels collecting full scan on the parent and metabolite ions, with isolation widths of 1 m/z. To quantify the amount of LasA/LasF in cell extracts, we generated a standard curve using external standards. Varying (known) amounts of purified LasA and LasF were quantified using the same LC–MS conditions as used for the cell extracts and linear regression was used to find the best-fit line, which was then used to estimate the amount of LasA/LasF in cell extracts. The limit of quantification for LasA was 34 ng ml^{-1}, and the

limit of detection for LasA was ~17 ng ml^{-1}; values for LasF were 26 ng ml^{-1} and ~10 ng ml^{-1}, respectively.

The amount of genomic DNA present in the cell extracts was taken as a measure of the number of cells to normalize the measurements of LasA and LasF across samples. (Note that the LasA/LasF ratio is an internally controlled value that should not depend on the number of cells collected for each sample and we present data in both ways in Fig. 3b,c.) For normalization, genomic DNA was extracted and quantitated from one-tenth of each cell sample; the remaining nine-tenths of each sample was used for LasA and LasF extraction.

Analysis of NCI-60 panel cell lines. The LasA toxicity data in NCI-60 cell lines was obtained from a previously published[3] study that reported data from the NCI Therapeutics Program, where LasA toxicity was measured in two similar experiments NSC: D-674673-X/0-1/17, Experiment ID: 9502RM14 and NSC: D-674673-X/0-1/35, Experiment ID: 9412MD01. The GI_{50} values from both the experiments were averaged for each cell line. NCI defines the GI_{50} as the drug concentration resulting in a 50% reduction in the net protein increase (as measured by sulforhodamine B staining) in control cells during the drug incubation. LDAH expression levels from RNA-seq were obtained from the Broad Institute's Cancer Cell Line Encyclopedia (CCLE). We obtained expression data for 45 cell lines out of the NCI-60 panel for which LasA toxicity data was also available. The LasA GI_{50} was plotted against the *LDAH* mRNA expression value (from CCLE) and the Pearson correlation coefficient was calculated using GraphPad Prism8.

RNA-seq analysis of serine hydrolases in Hap1 cells. Hap1 RNA-seq data has been reported in our previous publications[9] (NCBI GEO, accession number GSE75515). The RPKM values representing mRNA expression levels were obtained using Partek Flow software. The RPKM values of 117 metabolic serine hydrolases reported earlier[11,12] were plotted using GraphPad Prism8.

Fluorescence microscopy. The cells expressing eGFP-tagged LDAH were used to capture fluorescent images to study LDAH localization. The cells ($40–80 \times 10^3$ cells per well) were plated on an ibidi µ-Slide 8-Well plate. After 24 h the live cells were imaged using a Leica TCS SP8 confocal imaging system equipped with a 63× oil immersion objective and captured using the Leica Application Suite X software. For LipidTOX (Deep Red) staining, 40,000 Hap1 cells were plated in each well of an ibidi µ-Slide 8-Well plate. Cells were incubated with various small molecules for 24 h before fixation in 4% paraformaldehyde for 10 min at room temperature. LipidTOX (200 µl, 1:1,000 dilution in PBS) was added to the cells. The images were captured 45 min after addition of LipidTOX and processed using Fiji (ImageJ) software.

Statistics. Data analysis and data visualization were performed in GraphPad Prism8. The only exceptions were analysis of RNA-seq data, which was performed in Partek Flow, and analysis of screen data, which was performed using a published pipeline (code available at https://github.com/RohatgiLab/BAIMS-Pipeline). For LasA dose–response experiments, data were fit using the '[inhibitor] versus normalized response – variable slope' option in GraphPad Prism8 software, which uses the equation $y = 100/(1 + (IC_{50}/x)^{HillSlope})$. All values of IC_{50} shown in this paper are derived from these curve fits and include the standard error reported for these curve fits by GraphPad Prism8. Information about error bars, statistical tests and *n* values are reported in each figure legend and were calculated using GraphPad Prism8. All experiments were repeated at least three times with concordant results, with the exception of the experiment depicted in Fig. 5, which was repeated twice due to the scarcity of LasA.

Reporting Summary. Further information on research design is available in the Nature Research Reporting Summary linked to this article.

Data availability

The complete lists of the hits from the genetic screens are given in Supplementary Data 1. RNA-seq data from Hap1 cells is freely available at NCBI GEO, under accession no. GSE75515. The GI_{50} data for LasA and the RNA-seq data for cancer cell lines is publicly available (accession numbers given in the appropriate Methods section). Software for analysis of screen results has been described previously[9,10] and is freely available on github: https://github.com/RohatgiLab/BAIMS-Pipeline.

References

34. Ran, F. A. et al. Genome engineering using the CRISPR-Cas9 system. *Nat. Protoc.* **8**, 2281–2308 (2013).
35. Sanjana, N. E., Shalem, O. & Zhang, F. Improved vectors and genome-wide libraries for CRISPR screening. *Nat. Methods* **11**, 783–784 (2014).
36. Campeau, E. et al. A versatile viral system for expression and depletion of proteins in mammalian cells. *PLoS ONE* **4**, e6529 (2009).
37. Trost, B. M. et al. A concise synthesis of (−)-lasonolide A. *J. Am. Chem. Soc.* **136**, 88–91 (2014).

Acknowledgements

We thank D. Herschlag for bringing the LasA project to our attention, C. Pataki and R. Kopito for comments and advice on lipid droplet fractionation experiments and A. Lebensohn for advice on the project. The work was funded by DP2 GM105448 (R.R.), R35 GM118082 (R.R.), DP2 AI104557 (J.E.C.), American Heart Association Transformational Research Projects no. 18TPA34230103 (A.P.) and no. 18TPA34230086 (Y.-H.G.), and Dominic Ferraioli Foundation (A.P.). R.R. is a Josephine Q. Berry Faculty Scholar in Cancer Research at Stanford, J.E.C. is a David and Lucile Packard Foundation fellow and R.D. was supported by fellowships from the Stanford Dean's Fund and Alex's Lemonade Stand Foundation.

Author contributions

R.R. and R.D. designed the project. B.M.T. and C.E.S. designed and synthesized LasA, LasF, Ces-73, Ces-24a and Ces-24b. R.D. and J.E.C. executed the haploid genetic screens. R.D. and H.Q.N. performed the mass spectrometry experiments. R.D., A.P. and Y.-H.G. designed and constructed the LDAH variants. R.D. performed all other experiments and analyses presented in the paper. R.R. and R.D. wrote the paper and all the authors edited and commented on the paper.

Competing interests

The authors declare no competing interests.

Additional information

Supplementary information is available for this paper at https://doi.org/10.1038/s41589-019-0447-7.

Correspondence and requests for materials should be addressed to R.R.

Reprints and permissions information is available at www.nature.com/reprints.

nature research

Corresponding author(s): Rajat Rohatgi

Last updated by author(s): Nov 10, 2019

Reporting Summary

Nature Research wishes to improve the reproducibility of the work that we publish. This form provides structure for consistency and transparency in reporting. For further information on Nature Research policies, see Authors & Referees and the Editorial Policy Checklist.

Statistics

For all statistical analyses, confirm that the following items are present in the figure legend, table legend, main text, or Methods section.

n/a	Confirmed	
☐	☒	The exact sample size (*n*) for each experimental group/condition, given as a discrete number and unit of measurement
☐	☒	A statement on whether measurements were taken from distinct samples or whether the same sample was measured repeatedly
☐	☒	The statistical test(s) used AND whether they are one- or two-sided *Only common tests should be described solely by name; describe more complex techniques in the Methods section.*
☒	☐	A description of all covariates tested
☐	☒	A description of any assumptions or corrections, such as tests of normality and adjustment for multiple comparisons
☐	☒	A full description of the statistical parameters including central tendency (e.g. means) or other basic estimates (e.g. regression coefficient) AND variation (e.g. standard deviation) or associated estimates of uncertainty (e.g. confidence intervals)
☒	☐	For null hypothesis testing, the test statistic (e.g. *F*, *t*, *r*) with confidence intervals, effect sizes, degrees of freedom and *P* value noted *Give P values as exact values whenever suitable.*
☒	☐	For Bayesian analysis, information on the choice of priors and Markov chain Monte Carlo settings
☒	☐	For hierarchical and complex designs, identification of the appropriate level for tests and full reporting of outcomes
☐	☒	Estimates of effect sizes (e.g. Cohen's *d*, Pearson's *r*), indicating how they were calculated

Our web collection on statistics for biologists contains articles on many of the points above.

Software and code

Policy information about availability of computer code

Data collection	No software was used.
Data analysis	Graphpad Prism 8, ChemDraw Professional 16 and Microsoft Excel. For analysis of screen data, a previously described method was used (Dubey et al., Cancer Res. 2016, 76 (19), 5810-5821 and Carette et al., Nature 2011, 477, 340). The pipeline is freely available on github: https://github.com/RohatgiLab/BAIMS-Pipeline (as noted in the data/code availability statement in the manuscript).

For manuscripts utilizing custom algorithms or software that are central to the research but not yet described in published literature, software must be made available to editors/reviewers. We strongly encourage code deposition in a community repository (e.g. GitHub). See the Nature Research guidelines for submitting code & software for further information.

Data

Policy information about availability of data

All manuscripts must include a data availability statement. This statement should provide the following information, where applicable:

- Accession codes, unique identifiers, or web links for publicly available datasets
- A list of figures that have associated raw data
- A description of any restrictions on data availability

A data and code availability statement is now provided at the end of the manuscript. Most importantly, the complete results of the genetic screen is provided in the Supplementary Information.

Field-specific reporting

Please select the one below that is the best fit for your research. If you are not sure, read the appropriate sections before making your selection.

☒ Life sciences ☐ Behavioural & social sciences ☐ Ecological, evolutionary & environmental sciences

For a reference copy of the document with all sections, see nature.com/documents/nr-reporting-summary-flat.pdf

Life sciences study design

All studies must disclose on these points even when the disclosure is negative.

Sample size	No sample size calculation was performed; sample size was chosen such that statistical significance could be confidently established.
Data exclusions	No data were excluded from the analyses.
Replication	All attempts at replication were successful.
Randomization	Not applicable, there was no experimental group allocation.
Blinding	Not applicable, there was no experimental group allocation.

Reporting for specific materials, systems and methods

We require information from authors about some types of materials, experimental systems and methods used in many studies. Here, indicate whether each material, system or method listed is relevant to your study. If you are not sure if a list item applies to your research, read the appropriate section before selecting a response.

Materials & experimental systems

n/a	Involved in the study
☐	☒ Antibodies
☐	☒ Eukaryotic cell lines
☒	☐ Palaeontology
☒	☐ Animals and other organisms
☒	☐ Human research participants
☒	☐ Clinical data

Methods

n/a	Involved in the study
☒	☐ ChIP-seq
☒	☐ Flow cytometry
☒	☐ MRI-based neuroimaging

Antibodies

Antibodies used	Antibodies used are: anti-LDAH kindly provided by Dr. Antoni Paul from Albany Medical College; anti-GFP (NB600-308) from Novus Biologicals, Centennials, CO; anti-Calnexin (ADI-SPA-865-D) from Enzo Life Sciences, Farmingdale, NY; anti-ATGL (2138S) from Cell Signaling Technology, Danvers, MA; anti-αTubulin (T6199) from Sigma-Aldrich, St. Louis, MO.
Validation	Anti-LDAH was developed and reported previously by Dr. Antoni Paul (Arterioscler. Thromb. Vasc. Biol. 2014, 34 (2), 386-396.). It was further validated by showing that the band it detects on an immunoblot is lost when LDAH is genetically ablated by CRISPR editing. Anti-GFP (NB600-308), anti-Calnexin (ADI-SPA-865-D) and anti-ATGL (2138S) were validated by the respective vendors. Our additional validation has consisted of ensuring that the anti-GFP antibody does not detect an antigen in cells lacking GFP-fused proteins and by ensuring that the bands detected on an immunoblot are of the size expected for the corresponding antigen.

Eukaryotic cell lines

Policy information about cell lines

Cell line source(s)	MCF7 (ATCC Cat. # HTB-22); NCI-H1650 (ATCC CRL-5833); RKO (ATCC CRL-2577); A549 (ATCC CCL-185); HAP1 haploid human cells (kindly provided by Thijn Brummelkamp, now available from Horizon Discovery, Cambridge, United Kingdom) were derived and characterized as described previously (Carette, Raaben et al. 2011, Nature 477(7364): 340-343).
Authentication	MCF7, NCI-H1650, RKO and A549 were authenticated by ATCC. Low passages (<10) of the cells were used throughout the study, but further genetic testing of these lines was not performed in our laboratory. HAP1 cells (and derivatives) were validated by measuring their DNA content by propidium iodide staining. Genetically modified clonal derivatives were confirmed by sequencing of target loci and immuno-blotting when possible.

Mycoplasma contamination	The MCF7, NCI-H1650, RKO, A549 and HAP1 parent cell lines from which all other cell lines in the study were derived tested negative for mycoplasma contamination.
Commonly misidentified lines (See ICLAC register)	No commonly misidentified cell lines were used.